

Bond-order-wave phase and quantum phase transitions in the one-dimensional extended Hubbard model at half filling

Pinaki Sengupta

Department of Physics, University of Illinois at Urbana-Champaign, 1110 West Green Street, Urbana, Illinois 61801

Anders W. Sandvik

Department of Physics, Åbo Akademi University, Porthansgatan 3, FIN-20500, Turku, Finland

David K. Campbell

Departments of Physics and of Electrical and Computer Engineering, Boston University, 44 Cummington Street, Boston, Massachusetts 02215

(May 20, 2019)

We use a quantum Monte Carlo method to study the phase diagram of the one-dimensional extended Hubbard model at half filling for small to intermediate values of the on-site (U) and nearest-neighbor (V) repulsions. We confirm the existence of a novel, long-range-ordered bond-order-wave (BOW) phase recently predicted (M. Nakamura, J. Phys. Soc. Jpn. **68**, 3123 (1999)) in a small region of the parameter space between the familiar charge-density-wave (CDW) state for $V \gtrsim U/2$ and the state with dominant spin-density-wave (SDW) fluctuations for $V \lesssim U/2$. We discuss the nature of the transitions among these states and evaluate some of the critical exponents. Further, we determine accurately the position of the tricritical point, $(U_t, V_t) = (4.7 \pm 0.1, 2.51 \pm 0.02)$ (in energy units where the hopping integral is normalized to unity), above which the two continuous SDW-BOW-CDW transitions are replaced by one discontinuous (first-order) direct CDW-SDW transition. We also discuss advantages of using parallel tempering (or exchange Monte Carlo) — an extended ensemble method that we here combine with quantum Monte Carlo — in studies of quantum phase transitions.

PACS: 75.40.Gb, 75.40.Mg, 75.10.Jm, 75.30.Ds

I. INTRODUCTION

The one-dimensional (1D) extended Hubbard model has been extensively studied in recent years, both as an important theoretical test-bed for studying novel concepts in 1D (e.g., spin-charge separation) and methods, (e.g., quantum Monte Carlo, exact diagonalization, and the density matrix renormalization group) and as a useful model for several classes of quasi 1-D materials including copper-oxide materials related to the high-Tc cuprate superconductors,¹ conducting polymers² and organic charge-transfer salts.³ General 1D extended Hubbard models differ from the standard Hubbard model, which includes only an on-site electron-electron (e-e) interaction (U), by the addition of longer-range e-e interactions which are necessary to explain several experimentally observed effects in real materials, e.g., excitons in conducting polymers. The simplest extended Hubbard model (henceforth, EHM), on which we focus in this article, consists of adding a nearest neighbor e-e interaction V and is described by the Hamiltonian

$$\begin{aligned}
 H = & -t \sum_{i,\sigma} (c_{i+1,\sigma}^\dagger c_{i,\sigma} + h.c.) \\
 & + U \sum_i (n_{i,\uparrow} - \frac{1}{2})(n_{i,\downarrow} - \frac{1}{2}) \\
 & + V \sum_i (n_{i+1} - 1)(n_i - 1) + \mu \sum_i n_i, \quad (1)
 \end{aligned}$$

where $c_{i,\sigma}^\dagger (c_{i,\sigma})$ creates (annihilates) an electron with spin σ at site i , t is the hopping integral between adjacent sites, U and V are, respectively, the on-site and nearest neighbor interactions, and μ is the chemical potential. If the interaction parameters are assumed to arise solely from Coulomb interactions, both U and V are positive, and $U > V$. However, viewed as phenomenological parameters incorporating the effects of additional (e.g. electron-phonon) interactions, the ranges of these parameters can be much broader, including $U, V < 0$. Henceforth we set $t = 1$ and express the interaction parameters U and V in units of t .

The ground state phase diagram of the EHM at half filling ($\mu = 0$) has been extensively studied using both analytical and numerical methods. Despite the apparent simplicity of the model, the phase diagram shows surprisingly rich structure. In the limit $V=0$ (the standard Hubbard model), the Hamiltonian (1) can be diagonalized exactly using the generalized Bethe Ansatz.⁴ For $V \neq 0$, the model has been studied using perturbative methods and numerical simulations.⁵⁻¹³ Broadly, the phase diagram consists of insulating phases with dominant charge-density-wave (CDW) and spin-density-wave (SDW) characters and metallic phases where singlet and triplet superconducting correlations dominate. In the physically relevant region for "Coulomb-only" parameters ($U, V > 0$), the system is in a CDW phase for large V/U and in a state with dominant SDW fluctuations for small V/U . The CDW phase has broken discrete sym-

metry characterized predominantly by alternating doubly occupied and empty sites and exhibits long-range order. The SDW phase, on the other hand, has continuous symmetry and hence cannot exhibit long-range order in 1D (by the Mermin-Wagner theorem). Instead, it is a critical state characterized by the slow (algebraic) decay of the staggered spin-spin correlation function. Indeed, in the limit $U \gg V$, the model reduces to an effective Heisenberg model with $J \sim 1/(U - V)$. For small U and V ($U, V \ll 1$), the boundary between the CDW and the SDW phases was predicted to be at $U = 2V$ using weak coupling renormalization group techniques (“g-ology”)^{5,6} Strong coupling calculations using second-order perturbation theory also gave the same phase boundary ($U = 2V$) between the CDW and the SDW phases for large U and V ($U, V \gg 1$). For intermediate values of the parameters, the phase boundary was found to be shifted slightly away from the $U = 2V$ line such that the SDW phase is enhanced, as shown by quantum Monte Carlo simulations^{7,8} as well as strong coupling calculations using perturbation theory up to the fourth order.¹¹ Moreover, the nature of the transition is quite different in the two coupling regions, changing from continuous (second-order) in the weak coupling limit to discontinuous (first-order) in the strong coupling limit. Estimates for the location of the tricritical point, where the nature of the transition changes, have ranged from $U_t \simeq 1.5$ to $U_t \simeq 5$ (and $V_t = U_t/2$).^{7-10,13} Despite the broad uncertainty in the actual value of the tricritical point, the phase diagram was believed to be well understood.

Recently, however, by studying the EHM ground state broken symmetries using level crossings in excitation spectra obtained by exact diagonalization, Nakamura¹⁴ has argued for the existence of a novel bond-order-wave (BOW) phase for small to intermediate values of U and V in a narrow strip between the CDW and the SDW phases. The BOW phase is characterized by alternating strengths of the expectation value of the kinetic energy operator on the bonds. It is predicted to be a state where the discrete (two-fold) symmetry is broken and should hence exhibit true long-range order. Nakamura argues that the transition between CDW and SDW phases in this region is thus replaced two separate transitions: (i) a continuous transition from CDW to BOW; and (ii) a Kosterlitz-Thouless spin-gap transition from BOW to SDW. The BOW region vanishes at the tricritical point beyond which the transition between CDW and SDW phases is direct and discontinuous. A schematic phase diagram including Nakamura’s BOW state is shown in Fig. 1

Considering the long history of the 1D EHM and the large number of studies of the $U \approx 2V$ region with a variety of analytical and numerical tools, the proposal of a new phase is certainly remarkable. Importantly, the level crossing method used by Nakamura cannot by itself exclude the conventional scenario of a direct SDW-CDW transition for the whole range of $U, V > 0$; a level crossing corresponding to this transition was also found¹⁴ be-

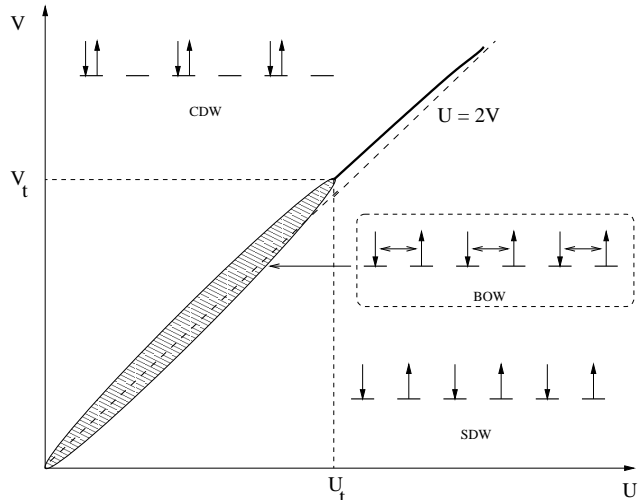


FIG. 1. Schematic ground state phase diagram of the EHM at half filling, as proposed by Nakamura. The CDW and BOW phases are long-range-ordered (broken-symmetry), whereas the SDW phase has no broken symmetry but exhibits an algebraically decaying spin-spin correlation function.

tween the SDW-BOW and BOW-CDW crossing curves. The position of the BOW-CDW level crossing is, however, in closer agreement with the strong-coupling result for the vanishing of the CDW order, and this was taken as evidence of a long-range-ordered BOW in the ground state for certain parameters. It is important to confirm this hitherto undiscovered phase using other methods.

To attempt this confirmation, we have used the highly efficient stochastic series expansion (SSE) quantum Monte Carlo method¹⁵⁻¹⁷ to study the EHM at half filling in the vicinity of $U = 2V$. This method allows us to probe directly the spin-charge- and bond-order correlations in the ground state of lattices with more than one hundred sites (up to 256 sites were used in this study). Using finite-size scaling techniques for the various order parameters, we confirm the existence of a BOW state with spin and charge gaps in a region very close to that predicted by Nakamura for small U, V . We also further improved the SSE simulations by applying a quantum version of the thermal parallel tempering scheme (or exchange Monte Carlo)¹⁸⁻²⁰ for simulations close to and across the phase boundaries. This “quantum parallel tempering” greatly reduced the effects of “sticking” — where the simulation gets trapped in the wrong phase close to a phase boundary — and was found to be particularly useful for the discontinuous (first order) direct CDW-SDW transition. As a consequence, we were able to obtain a more accurate estimate for the location of the tricritical point (U_t, V_t) where the BOW phase vanishes and is replaced by a first-order SDW-CDW transition line. As we discuss below, we find $U_t = 4.7 \pm 0.1$, $V_t = 2.51 \pm 0.02$.

The remainder of the paper is organized into three sections and two appendices. In Sec. II we briefly sketch the SSE method and introduce the different observables we

study. In Sec. III we present the results of our simulations and discuss their interpretation. In Sec. IV we conclude with a brief summary and suggestions for related future work. In Appendix A, we present some important details of the extension of the prior SSE method to allow efficient loop updates for fermions. We illustrate the advantages of the quantum parallel tempering scheme in Appendix B.

II. NUMERICAL METHODS AND OBSERVABLES

A. The SSE method and its fermion loop-update extension

The SSE method^{15,16} is a finite-temperature quantum Monte Carlo method based on importance sampling of the diagonal elements of the Taylor expansion of $e^{-\beta H}$, where β is the inverse temperature $\beta = t/T$. Ground state expectation values can be obtained using sufficiently large values of β , and there are no approximations beyond statistical errors. Recently, in the context of spin systems,¹⁷ an efficient “operator loop update” was developed to sample the operator sequences appearing in the expansion. The resulting method has proven to be very efficient.^{21,22} To apply the most efficient variant of SSE method to the EHM, we need to generalize the previous operator loop update scheme to spinful fermions. This is an important extension, but because of its highly technical nature we have relegated our detailed discussion of it to an appendix.

We have applied the SSE algorithm to the 1D EHM for system sizes ranging from $N = 16$ to 256 sites, with maximum inverse temperatures β chosen appropriately to isolate the ground state. Although the operator-loop update is indeed significantly more efficient than previous local updates for sampling of the SSE configurations, we still have problems with “trapping” close to a first order phase transition, i.e., the simulation can get stuck in the wrong phase very close to the critical point. There are also problems with slow dynamics in long-range ordered phases with a broken discrete symmetry (such as BOW or CDW phases). In order to overcome these problems we have developed a “quantum parallel tempering” scheme — a generalization of the thermal parallel tempering method^{18–20} commonly used to equilibrate classical spin glass simulations. The method amounts to running several simulations on a parallel computer, using a fixed value of U and different closely spaced values of V at and around the critical value V_c . Along with the usual Monte Carlo updates, we attempt to swap the configurations for processes with adjacent values of V at regular intervals (typically after every Monte Carlo step) according to a scheme that maintains detailed balance in the space of the parallel simulations, as explained in Appendix B. In contrast to Ref. 18, we find parallel tem-

pering to be particularly useful in the study of the first-order transition, where the problem of trapping is the most pronounced. In Appendix B we also present a comparative example to illustrate the improvement obtained by parallel tempering.

B. Observables

In addition to the ground state energy, $E = \langle H \rangle / N$, the observables we study include the static structure factors and susceptibilities corresponding to the different phases (CDW, SDW and BOW). The structure factors are given by

$$\begin{aligned} S_{CDW}(q) &= \frac{1}{N} \sum_{i,j} e^{iq(i-j)} \langle n_i n_j \rangle - \langle n_i \rangle^2, \\ S_{SDW}(q) &= \frac{1}{N} \sum_{i,j} e^{iq(i-j)} \langle S_i^z S_j^z \rangle, \\ S_{BOW}(q) &= \frac{1}{N} \sum_{i,j,\sigma} e^{iq(i-j)} \langle K_i K_j \rangle - \langle K_i \rangle^2, \end{aligned} \quad (2)$$

where

$$K_i = \sum_{\sigma=\uparrow,\downarrow} (c_{i+1,\sigma}^\dagger c_{i,\sigma} + h.c.) \quad (3)$$

is the kinetic energy operator associated with the i^{th} bond. The corresponding static susceptibilities are given by

$$\chi_{SDW}(q) = \frac{1}{N} \sum_{i,j} e^{iq(i-j)} \int_0^\beta d\tau \langle S_i^z(\tau) S_j^z(0) \rangle \quad (4)$$

and analogous expressions for $\chi_{CDW}(q)$ and $\chi_{BOW}(q)$. Since all the phases mentioned have a period 2, the staggered structure factor and susceptibilities are the most important observables. We define order parameters for the phases in terms of the staggered structure factors:

$$m_\alpha = \sqrt{S_\alpha(\pi)/N}, \quad (5)$$

where $\alpha = \text{CDW, SDW, or BOW}$. We have also studied the charge stiffness constant, ρ_c . It is defined as the second derivative of the internal energy per site, E , with respect to a twist, ϕ ,²³

$$\rho_c = \frac{\partial^2 E(\phi)}{\partial \phi^2}, \quad (6)$$

under which the hopping term in the Hamiltonian (1) is replaced by

$$K_c(\phi) = -t \sum_{i,\sigma} (e^{-i\phi} c_{i+1,\sigma}^\dagger c_{i,\sigma} + h.c.). \quad (7)$$

The spin stiffness constant, ρ_s , is defined by a similar expression, with the hopping term now being replaced by

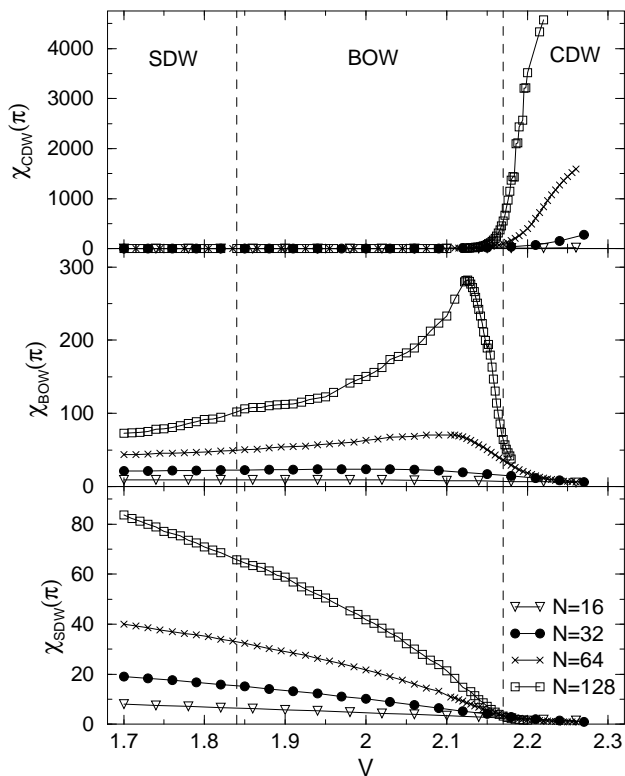


FIG. 2. The variation with V (at fixed $U = 4$) of the staggered susceptibilities (CDW, BOW, and SDW, from the top) in the neighborhood of the BOW phase predicted by Nakamura (the vertical dashed lines show the predicted SDW-BOW and BOW-CDW boundaries). The statistical errors are typically of the order of the size of the symbols (slightly larger for the $N = 128$ CDW at high V). The scans for $N = 16$ and 32 were obtained in single parallel tempering simulations, whereas those for $N = 64$ and 128 consisted of 2 and 4 non-overlapping runs, respectively.

$$K_s(\phi) = -t \sum_{i,\sigma} (e^{-i\phi_\sigma} c_{i+1,\sigma}^\dagger c_{i,\sigma} + h.c.), \quad (8)$$

with $\phi_\uparrow = -\phi_\downarrow = \phi$. In the framework of the SSE method, the estimators for the charge and spin stiffness are given in terms of expectation values of squared winding numbers (see Appendix A).

III. RESULTS

As noted above, we have studied chains of lengths $N = 16$ to $N = 256$ with periodic boundary conditions.²⁴ Typically, an inverse temperature of $\beta = 2N$ was sufficient for the calculated properties to have converged to their ground state values, except $N = 256$, for which $\beta = 4N$ was needed for some quantities. In this section we first discuss our evidence for the existence of a long-range BOW phase, then our analysis of the continuous BOW-CDW transition for small (U, V) and the discontinuous SDW-CDW transitions for large (U, V), and finally

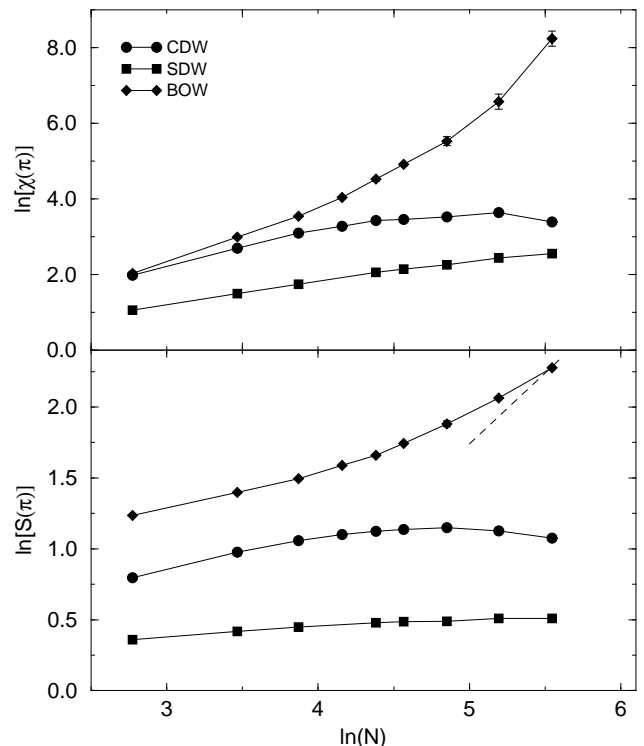


FIG. 3. $\ln[\chi(\pi)]$ and $\ln[S(\pi)]$ vs $\ln[N]$ for the different phases at $U = 4.0$, $V = 2.14$ and system sizes N up to 256. The dashed line in the $S(\pi)$ panel has slope 1.

our determination of the location of the tricritical point separating these two transitions.

A. Existence of the BOW phase

Plots of the variation of the staggered susceptibilities corresponding to the three different phases — CDW, SDW, and BOW — show the existence of strong BOW fluctuations in a region with $V \simeq U/2$ in parameter space where Nakamura predicted a BOW state. Fig. 2 is such a plot for $U = 4.0$ and $1.7 \leq V < 2.3$. In a long-range ordered phase (BOW, CDW), the corresponding $\chi(\pi)$ is expected to diverge with increasing system whereas the other two susceptibilities should converge to constants. In the SDW phase there is no long-range order but algebraically decaying correlations of both SDW and BOW nature; hence $\chi_{SDW}(\pi)$ and $\chi_{BOW}(\pi)$ should both diverge here, but the BOW divergence should be much slower than in the long-ranged BOW phase. These behaviors are indeed seen in Fig. 2, with the susceptibilities for SDW, BOW, and CDW dominating in turn as V is increased. The BOW-CDW phase boundary can be quite well resolved since it involves a standard second order (continuous) phase transition. On the other hand, the SDW-BOW boundary is more difficult to locate, for it involves a Kosterlitz-Thouless transition in which the spin gap opens exponentially slowly as one enters the BOW

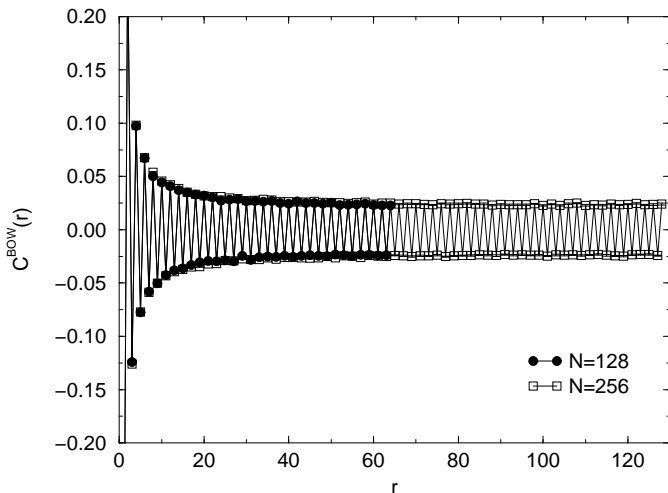


FIG. 4. The real-space BOW correlation function at $U = 4.0$, $V = 2.14$ for system sizes $N = 128$ and 256 .

phase,¹⁴ resulting in only a slow decay of the staggered SDW susceptibility in the BOW phase for the system sizes accessible in our work.

Fig. 3 shows $\ln[\chi(\pi)]$ and $\ln[S(\pi)]$ versus $\ln[N]$ for the parameters $(U, V) = (4.0, 2.14)$ for which the ground state should be inside the BOW phase. We find that both $\chi_{BOW}(\pi)$ and $S_{BOW}(\pi)$ diverge strongly with system size, whereas the structure factor and susceptibility corresponding to CDW have a maximum and then decrease with system size for large N . The SDW structure factor appears to have converged for $N = 256$ but the susceptibility still shows a weak growth — in a spin-gapped BOW phase it should eventually converge, too, but if the gap is very small the convergence occurs only for much larger systems. In any case, the growth is much slower than N , which should be the asymptotic behavior in an SDW phase for any spin-rotationally invariant 1D system,²⁵ and hence an asymptotic divergence of $\chi_{SDW}(\pi)$ can be excluded. The dominant asymptotic characteristic of the ground state is clearly BOW. The system sizes considered are not large enough for $S_{BOW}(\pi)$ to have reached the asymptotic behavior $\sim N$ expected if there is long-range order, but we see a clear approach to such behavior. The very fast divergence of $\chi_{BOW}(\pi)$ is expected on account of the two-fold degenerate BOW ground state. For finite N this degeneracy is not perfect, but an exponentially fast closing of the gap between the symmetric and antisymmetric linear combinations of the two asymptotically degenerate symmetry-broken ordered states can be expected, which would eventually cause $\chi_{BOW}(\pi)$ to diverge exponentially.

The most direct evidence for a long-range BOW comes from the the real-space kinetic energy correlation function

$$C^{BOW}(r) = \langle K_i K_{i+r} \rangle - \langle K_i \rangle^2. \quad (9)$$

As seen in Figure 4, this correlation function oscillates

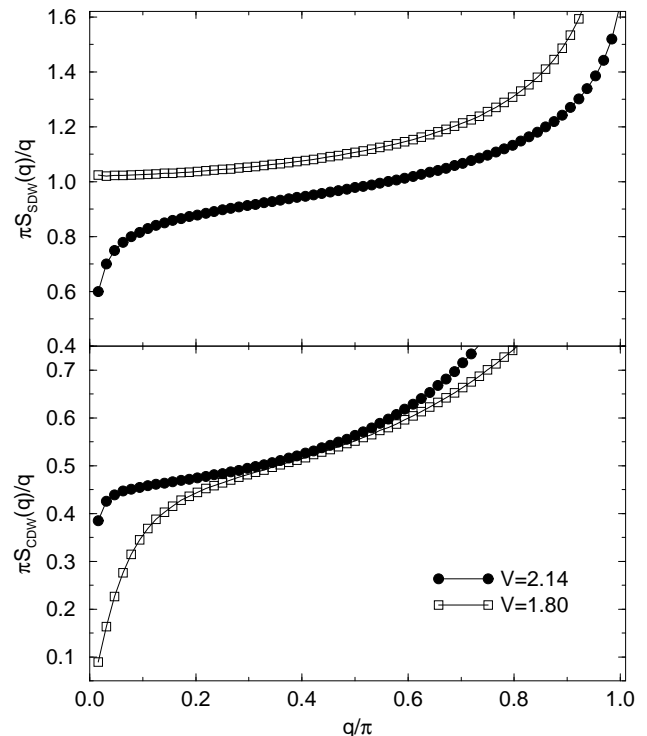


FIG. 5. $S_{SDW}(q)/q$ and $S_{CDW}(q)/q$ vs q for $U = 4.0$ and $V = 2.14$ and $V = 1.8$ ($N = 128$).

with period 2 and its magnitude decays considerably for short distances. For long distances there is a convergence to a constant, non-zero magnitude, which is the same within statistical errors for $N = 128$ and 256 . The significant enhancement of the correlations at short distances explain the deviations from the asymptotic linear scaling of the integrated correlation function, $S_{BOW}(\pi)$, in Figure 3.

Further proof of the existence of the BOW phase is obtained by looking for spin and charge gaps in this region. Instead of calculating the gaps directly, which can not easily be done to high accuracy for large system sizes, we use the following indirect method: It is known²⁵ that if the ground state of a 1D system is gapless in the spin sector, the correlation exponent governing the asymptotic equal-time spin correlation function, $K_\sigma = 1$. It has been further shown²⁶ that the slope $S_{SDW}(q)/q$ gives K_σ/π in the limit $q \rightarrow 0$. Hence, $S_{SDW}(q)/q \rightarrow 1/\pi$ as $q \rightarrow 0$. On the other hand, if the ground state has a spin gap, $S_{SDW}(q)/q \rightarrow 0$ as $q \rightarrow 0$. With this criterion even a very small spin gap can be detected, since it is in practice sufficient to see that $S_{SDW}(q)/q$ decays below $1/\pi$ for small q to conclude that $K_\sigma \neq 1$ and hence that a spin gap must be present. Similarly, for a ground state with no charge gap, $S_{CDW}(q)/q \rightarrow K_\rho/\pi$ as $q \rightarrow 0$ whereas if the ground state does have a charge gap, $S_{CDW}(q)/q \rightarrow 0$ as $q \rightarrow 0$. Unlike K_σ , where the value is fixed at 1 for spin rotationally invariant systems, K_ρ is a function of U and V , and its precise value for given U and V is not

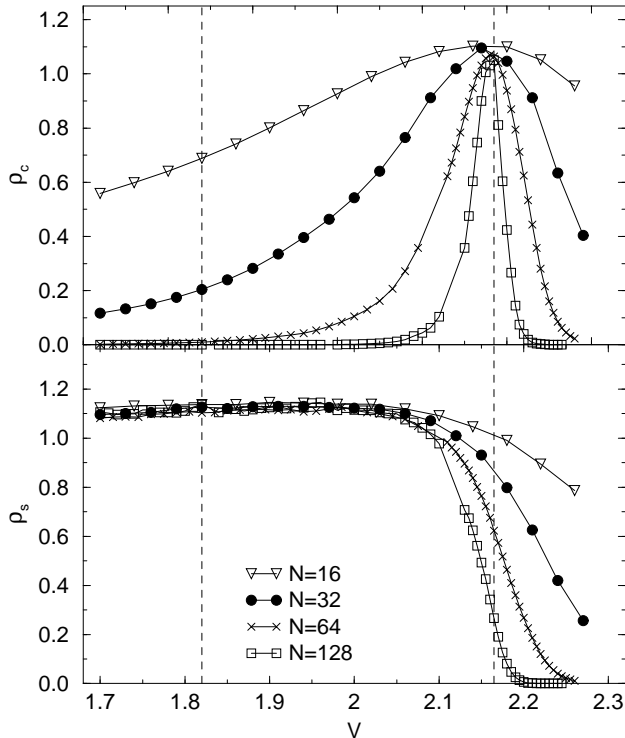


FIG. 6. Behavior of the charge and spin stiffness across the CDW-BOW boundary for $U = 4$. The upper(lower) panel shows the charge(spin) stiffness. The vertical dashed lines indicate the position of the phase boundaries according to Nakamura.

known (except for $V = 0$ ²⁷). Fig. 5 shows $\pi S_{SDW}(q)/q$ and $\pi S_{CDW}(q)/q$ versus q/π for $U = 4.0$ and two values of V . One of the points ($V = 2.14$) is inside the BOW phase, whereas the other ($V = 1.8$) is in the SDW phase. The $\pi S_{SDW}(q)/q$ curve for $V = 1.8$ is close to 1 for a wide range of q values and decays slowly²⁸ towards 1 whereas the $V = 2.14$ curve exhibits a sharp drop as $q \rightarrow 0$ indicating, respectively, the absence and the presence of a spin gap. Similarly, the evidence for a vanishing limit of $S_{CDW}(q)/q$ and hence of a charge gap for $V = 1.8$ is clear. Since the point $V = 2.14$ is quite close to the critical point ($V_c = 2.16$) where the charge gap vanishes, the magnitude of the charge gap is very small and we need to go to still smaller q , i.e., larger system size, to see a pronounced effect like that for $V = 1.8$. Nevertheless, the downturn for the smallest q is a good indication of a gap.

The opening of spin and charge gaps can also be detected in the spin and charge stiffness constants, which should vanish as $N \rightarrow \infty$ if there are gaps. The asymptotic charge stiffness should hence be non-zero only exactly at the CDW-BOW phase boundary. The spin stiffness should be non-zero in the SDW phase, should vanish at the BOW-SDW phase boundary²⁹ and remain zero inside the CDW phase. In Fig. 6 we show the charge stiffness for $U = 4.0$ in the neighborhood of the CDW-BOW boundary. As expected, the charge stiffness peaks

at the phase boundary and decreases rapidly away from it, confirming the vanishing of the charge gap only at the CDW-BOW phase boundary. The spin stiffness is clearly zero in the CDW phase, and a sharp decrease with increasing N is also seen for V values well inside the BOW phase. Since the spin gap opens up exponentially slowly at the BOW-SDW boundary it is difficult to locate the transition this way. Our data nevertheless indicate that the BOW phase at $U = 4$ does not extend down to the value $V \approx 1.82$ obtained by Nakamura. Comparing the behavior of the spin stiffness with that of a spin-phonon model with a similar spin gap transition,³⁰ we estimate that the critical V is within the range $2.00 - 2.05$.

Hence, for $U = 4$ we have confirmed, using several different observables, that there is a range of V values, from ≈ 2.0 to $V = 2.16$ where there is long-range BOW order and gaps for both spin and charge excitations.

B. The BOW-CDW transition

In addition to proving the existence of the BOW phase, we have studied in detail the nature of the continuous (second-order) CDW-BOW transition for two different values of U ($U < U_t$). For $(U, V) = (U_c, V_c)$, i.e., on the CDW-BOW phase boundary, the real space staggered charge and kinetic energy correlation functions fall off algebraically as

$$\begin{aligned} \langle n_i n_{i+r} \rangle (-1)^r &\sim r^{-\eta}, \\ (\langle K_i K_{i+r} \rangle - \langle K_i \rangle^2) (-1)^r &\sim r^{-\eta}. \end{aligned} \quad (10)$$

Based on conformal field theory calculations for similar phase transitions in 1D spin systems,³¹ the exponent η can be expected to depend on (U_c, V_c) but should be the same for both the CDW and BOW correlations. This gives the finite-size scaling of the structure factor and the susceptibility at the critical point:

$$\begin{aligned} S_{CDW, BOW}(\pi) &\sim N^{1-\eta}, \\ \chi_{CDW, BOW}(\pi) &\sim N^{2-\eta}. \end{aligned} \quad (11)$$

Fig. 7 presents plots of $\ln[\chi_{CDW}]$ and $\ln[\chi_{BOW}]$ versus $\ln[N]$ for $U = 4.0$ and three different values of V around the critical point, which as discussed above should be close to 2.16. The data points for $V = 2.16$ indeed fall almost on straight lines, indicating critical scaling for both the CDW and BOW fluctuations. The value of the critical exponent η , obtained from the slope of the $V = 2.16$ curves for both χ_{CDW} and χ_{BOW} is $\eta = 0.47 \pm 0.05$. The scaling of the structure factors, S_{CDW} and S_{BOW} , at $V = 2.16$ is also consistent with $\eta \approx 0.47$. Hence, all data are in complete agreement with $V_c \approx 2.16$ and a single exponent η in Eq. (11). A similar analysis for $U = 3.0$ yields a critical value $V_c = 1.65$ (again in complete agreement with Nakamura's result). The critical exponent is $\eta = 0.9 \pm 0.1$. An exponent that varies continuously with the parameters is expected for a phase

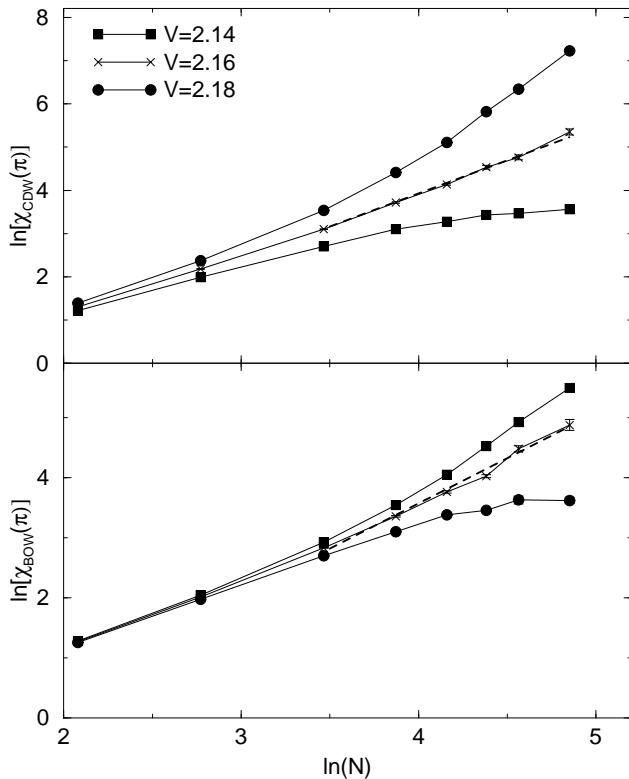


FIG. 7. $\ln[\chi_{CDW}(\pi)]$ and $\ln[\chi_{BOW}(\pi)]$ vs. $\ln[N]$ for $U=4.0$ and different values of V near the critical point. The dashed lines are fits to the $V = 2.16$ data.

transition belonging to the class of $c = 1$ conformal field theories.^{31,32}

C. First-order SDW-CDW transition

For $U > U_t$, the transition is a discontinuous (first-order) direct CDW-SDW transition with no intervening BOW phase. Fig. 8 shows the V dependence of the CDW order parameter, the total energy, and the kinetic energy across the phase boundary for $U = 8.0$, which according to previous studies^{7-10,13} should be well within the regime of first-order transitions. The characteristics of a first-order transition are indeed quite apparent. The order parameter and the kinetic energy change rapidly at the transition point, $V_c \approx 4.14$. The finite-size effects diminish with increasing N as the results approach the limiting behavior of a discontinuity in the order parameter and the kinetic energy in the thermodynamic limit. The total energy remains continuous, but there is a clear break in slope at the transition.

The size dependence of the BOW order-parameter is shown in Fig. 9. It becomes considerably smaller inside the CDW phase than before the transition. This is expected, since in the SDW phase, but not in the CDW phase, there should be power-law decaying BOW correlations. The BOW order parameter decays rapidly with the

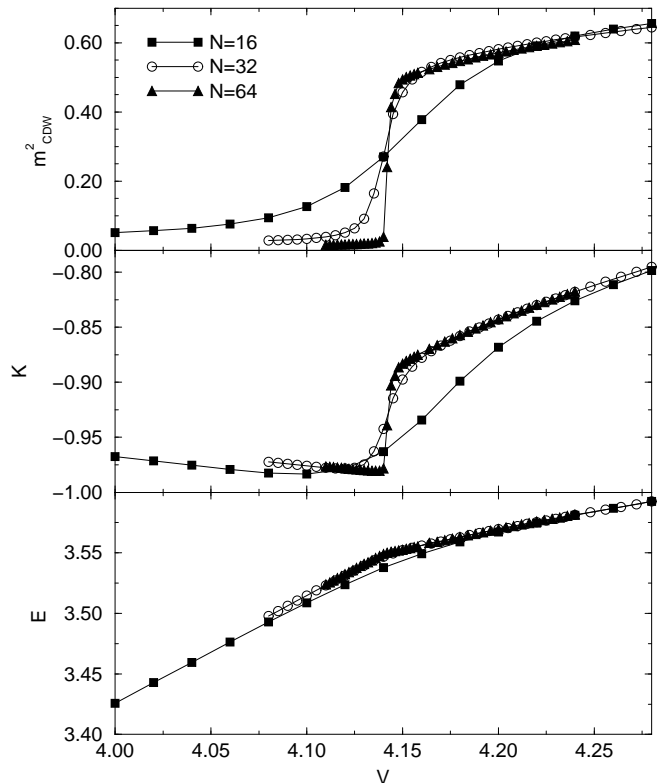


FIG. 8. The behavior of the CDW order parameter, the kinetic energy and the ground state energy across the SDW-CDW transition for various system sizes and $U = 8.0$.

system size, however, confirming that there is no long-range BOW for this $U > U_t$.

The behavior with increasingly sharp discontinuities seen in Fig. 8 indicates a first-order transition due to an avoided level crossing. Note that with increasing chain length the CDW order parameter approaches its thermodynamic value from above for $V < V_c$ and from below for $V > V_c$. The curves for different system sizes cross one another in the neighborhood of $V = V_c$ and then once again for a higher V . The second crossing point moves down towards the first one as N increases, whereas the first crossing does not change much with V and appears to be a good criterion for locating the transition point.

The two curve crossings can be understood as follows: In a transition caused by an avoided level crossing, a crossing of the order parameter curves close to the critical coupling (approaching the critical coupling as $N \rightarrow \infty$) can be expected since the low-energy levels corresponding to an ordered and disordered state swap characters within a parameter range $V \pm \Delta_V(N)$, with $\Delta_V(N) \rightarrow 0$ as $N \rightarrow \infty$. This behavior is seen clearly in Fig. 8. The finite- N ground state starts to develop CDW characteristics at $V - \Delta_V(N)$ and thus, for a fixed $V < V_c$, the CDW order parameter decreases with increasing N . An analogous argument for fixed $V > V_c$ close to V_c gives that in this case the CDW order must increase with increasing N . On the other hand, for $V \gg V_c$ the real-space

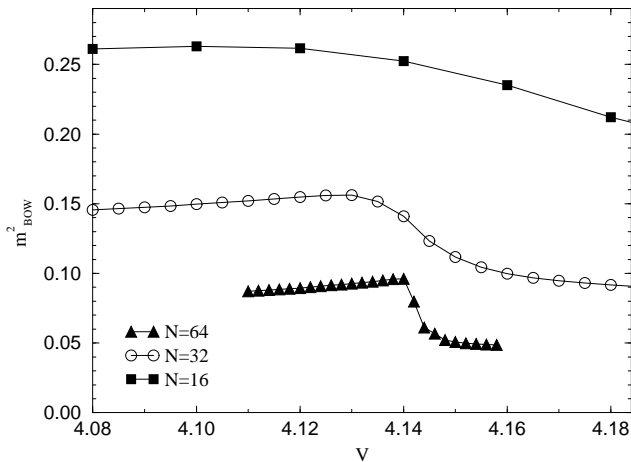


FIG. 9. The behavior of the BOW order parameter across the SDW-CDW transition for various system sizes and $U = 8.0$.

CDW correlations are enhanced at short distances (in the same way as the BOW correlations shown in Fig. 4) and for small system sizes there is also some enhancement of the long-distance correlations due to the periodic boundary conditions. Hence, one can expect the CDW order parameter, when defined and measured in terms of its squared expectation Eq. (5), to *decrease* with N for $V \gg V_c$ and this explains the second crossing of the order parameter curves seen in Fig. 8.

D. Tricritical point

Although the existence of the tricritical point has long been known, its location in the (U, V) plane has not previously been determined accurately using large system sizes. Hirsch^{7,8} estimated a value of $U_t = 3$ using world line Monte Carlo. Cannon and Fradkin⁹ obtained $U_t = 1.5$ using field theory techniques and world lines. Later Cannon, Scalettar and Fradkin¹⁰ obtained a value of $U_t = 3.5 - 5$ using finite-size scaling of Lanczos results. Using a combination of bosonization and RG techniques, Voit¹³ obtained $U_t = 4.76$. However, as Voit himself pointed out, the validity of bosonization and RG, which are applicable in the limit $U, V \rightarrow 0$, for intermediate values of the parameters is *a priori* questionable.

By using larger system sizes and an alternative criterion to distinguish between a continuous transition and a first-order level crossing transition, we have obtained an estimate of the tricritical point that we consider more accurate and reliable than the previous estimates. In contrast to most previous numerical studies, our method is not based on plotting histograms of the order parameter (although such histograms certainly can also be generated with our methods). Instead we exploit the qualitatively different finite-size dependence of the growth of the order parameter close to the transition above and below the tricritical point. The order parameter curves for dif-

ferent system sizes cross each other at or very close to the critical point ($V = V_c$) in the case of a first order transition, as discussed above in Sec. III-C. Such a crossing cannot occur for a second order transition, where instead there should be finite-size scaling governed by Eq. (11). This qualitative difference in the finite-size dependence of the order parameter close to the transition point above and below the tricritical point leads us to expect that in the neighborhood of the tricritical point, the plot of the order parameter for different chain lengths will closely coincide with one another close to $V = V_c$, and V_c is the point at which the curves barely touch each other. When the system size becomes sufficiently large one can also directly observe discontinuities developing, in the order parameter as well as in other quantities, as in Fig. 8, but in practice this is not possible very close to the transition. The phenomenon of barely intersecting curves can be observed even for moderate system sizes, however.

Fig. 10 shows the finite-size dependence of the CDW order parameter across the transition for 3 different values of U close to our estimated tricritical point. For $U = 4.2$, only the $N = 16$ curve crosses the other curves, and this happens far from the critical point. The non-crossing for larger system sizes show that the transition must be second order at this U . For $U = 5.2$ all curves show crossing behavior and a discontinuity can also be seen developing for the largest system size, i.e., the transition is here of first order. The curves for $U = 4.6$ closely follow the expected behavior at the tricritical point, with the curves for the largest systems barely touching each other. Based on data also for other values of U we estimate the tricritical point to be $(U_t = 4.7 \pm 0.1, V_t = 2.51 \pm 0.02)$. This agrees surprisingly well with Voit's estimate ($U_t = 4.76$).¹³ However, it is not clear whether this agreement is fortuitous or whether there is some underlying symmetry that renders bosonization and RG (that assume $U, V \ll 1$) applicable close to the tricritical point.

IV. SUMMARY

To summarize, we have studied the 1D EHM using the SSE method incorporating an efficient operator-loop update and a parallel tempering scheme. Our results confirm the surprising prediction¹⁴ of the existence of a novel long-range-ordered BOW phase between the well-known CDW and SDW phases in the ground state phase diagram for small to intermediate values of the on-site interaction U ($U < U_t$). We have presented several ways to detect the spin and charge gaps expected in the BOW phase and have also probed directly the BOW correlations and concluded that true long-range order develops. We have studied a few points on the BOW-CDW phase boundary and obtained a very good agreement with Nakamura's level crossing prediction¹⁴ for the location of this phase boundary. For the SDW-BOW phase

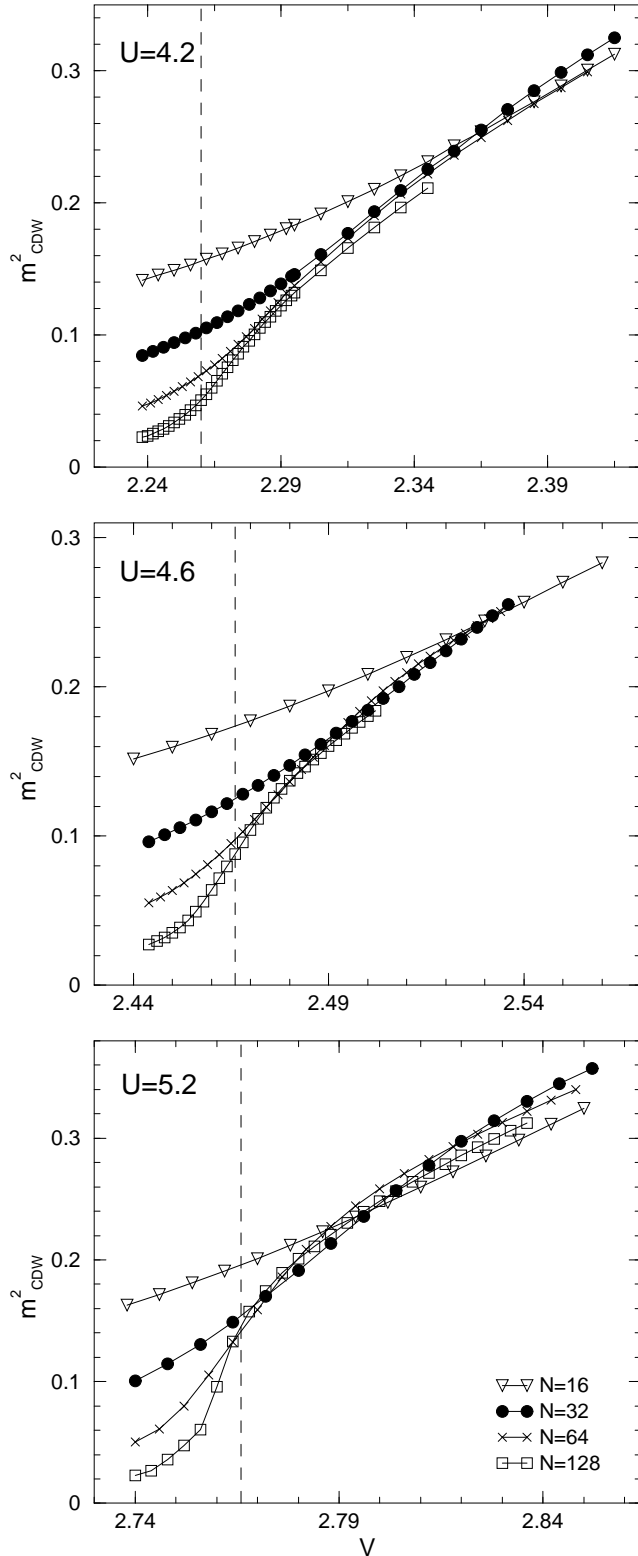


FIG. 10. The CDW order parameter vs V across the BOW-CDW boundary for several system sizes near the tricritical point. The dashed line shows the position of V_c for the respective U s, extracted using the peak position of the charge stiffness (see Fig. 6).

boundary, our results indicate a higher critical V for fixed U than given by the level crossing method¹⁴ and thus over-all a slightly smaller size of the BOW phase. Our results are for significantly larger systems than in the previous study and it is not surprising that the finite-size effects in the level crossings can be large for the SDW-BOW transition since the spin gap opens exponentially slowly in this Kosterlitz-Thouless transition. An over-estimation of the size of the BOW phase from the level crossings is also apparent considering that our estimated tricritical point is well within the BOW phase of Nakamura's phase diagram. Since our BOW-CDW phase boundaries agree, this indicates problems with the scaling of the exact SDW-BOW level crossings close to the tricritical point, as was also mentioned by Nakamura.¹⁴

We have studied the continuous (second-order) CDW-BOW transition in detail using finite-size scaling analysis for two different values of U and the corresponding critical values of V . The non-constant values of the calculated critical exponent η indicate that the transition belongs to the class of $c = 1$ conformal field theories, where the critical exponents vary continuously with the parameters.^{31,32} For large values of U ($U > U_t$) the transition is discontinuous (first-order). We have shown that curves of the CDW order parameter across this boundary for different system sizes cross each other twice, and explained this behavior in terms of an avoided level crossing. We have also used the curve crossings as a means to locate the position of the tricritical point with far greater accuracy than previously attained. Our estimate for the tricritical point is $U_t = 4.7 \pm 0.1$, $V_t = 2.51 \pm 0.02$.

An interesting question naturally arises from the existence of the Nakamura BOW phase: Can the EHM model support a soliton lattice when doped slightly away from half-filling? It has been believed that couplings to phonons, e.g., in the Su-Schrieffer-Heeger model,³³ would be needed for such an insulating state to exist before the system becomes metallic at higher doping levels. It is possible that a state of immobile defects could develop also from the Nakamura BOW phase, without phonons. We plan to address this issue in future work.

ACKNOWLEDGMENTS

We would like to thank R. T. Clay for discussions of the operator-loop update for fermions. A.W.S. would like to thank O. Sushkov for discussions. This work was supported by the NSF under grant No. DMR-97-12765. Most of the numerical calculations were carried out on the SGI Origin2000 and Condor systems at the NCSA, Urbana, Illinois. Some of the simulations were carried out on the Origin2000 at the Center for Scientific Computing in Helsinki.

APPENDIX A: OPERATOR-LOOP UPDATES IN THE SSE METHOD.

The basic SSE approach has been discussed in several papers.^{15–17} We here start with brief review as a basis for introducing the operator-loop update¹⁷ in the context of fermion models.

To implement the SSE method, the Hamiltonian (1) is written, upto an additive constant, in the form

$$H = - \sum_{b(i)=1}^N (H_{1,b(i)} + H_{2,b(i)} + H_{3,b(i)}), \quad (\text{A1})$$

where b is the bond connecting the sites b and $b+1$, N is the length of the chain, and the operators $H_{a,b}$, $a = 1, 2, 3$ are defined as

$$\begin{aligned} H_{1,b} &= C - \frac{U}{2} [(n_{b,\uparrow} - \frac{1}{2})(n_{b,\downarrow} - \frac{1}{2}) \\ &\quad + (n_{b+1,\uparrow} - \frac{1}{2})(n_{b+1,\downarrow} - \frac{1}{2})] \\ &\quad - V(n_i - 1)(n_{b+1} - 1), \quad (\text{A2}) \\ H_{2,b} &= t(c_{b+1,\downarrow}^\dagger c_{b,\downarrow} + h.c.), \\ H_{3,b} &= t(c_{b+1,\uparrow}^\dagger c_{b,\uparrow} + h.c.). \end{aligned}$$

The constant C shifts the zero of the energy and is chosen to ensure a non-negative expectation value for $H_{1,b}$ (needed in order to ensure a positive definite expansion of the partition function). Introducing a basis $\{|\alpha\rangle\} = \{|\zeta_1, \zeta_2, \dots, \zeta_N\rangle\}$, where $\zeta_i \in \{0, \uparrow, \downarrow, \uparrow\downarrow\}$ denotes the electron state at the site i , the partition function $Z = \text{Tr}\{e^{-\beta H}\}$ can be expanded in a Taylor series as

$$Z = \sum_{\alpha} \sum_{n=0}^{\infty} \sum_{S_n} \frac{\beta^n}{n!} \langle \alpha | \prod_{p=1}^n H_{a_p, b_p} | \alpha \rangle, \quad (\text{A3})$$

where S_n denotes a sequence of index pairs defining the operator string $\prod_{p=1}^n H_{a_p, b_p}$:

$$S_n = [a, b]_1 [a, b]_2 \dots [a, b]_n, \quad (\text{A4})$$

where we use the notation $[a, b]_p = [a_p, b_p]$ and $a \in \{1, 2, 3\}$, $b \in \{1, \dots, N\}$. In order to construct an efficient updating scheme, the Taylor series is truncated at a self-consistently determined power L , large enough to cause only an exponentially small, completely negligible error ($L \sim \beta E$, where E is the total internal energy; for details see Refs. 15,16). We can then define a sampling space where the length of the sequences is fixed, by inserting $L - n$ unit operators, denoted by $H_{0,0}$, into each sequence. The terms in the partition function must be divided by $\binom{L}{n}$ in order to compensate for the different ways of inserting the unit operators. The summation over n is then implicitly included in the summation over all sequences of length L . The partition function now takes the form

$$Z = \sum_{\alpha} \sum_{S_L} \frac{\beta^n (L-n)!}{L!} \langle \alpha | \prod_{p=1}^L H_{a_p, b_p} | \alpha \rangle, \quad (\text{A5})$$

where the operator-index pairs $[a, b]_p$ in (A4) with $n = L$ now have $a \in \{1, 2, 3\}$ and $b \in \{1, \dots, N\}$ or $[a, b]_p = [0, 0]$. For convenience, we introduce a notation for states obtained by the action of the first p elements of the operator string S_L :

$$|\alpha(p)\rangle \sim \prod_{j=1}^p H_{a_j, b(i)_j} |\alpha\rangle. \quad (\text{A6})$$

For a nonzero contribution to the partition function, $|\alpha(L)\rangle = |\alpha(0)\rangle$.

A Monte Carlo scheme is used to sample the configurations (α, S_L) according to their relative contributions (weights) to Z . The sampling scheme consists of two types of updates^{15–17}, referred to as diagonal update and operator-loop updates. The diagonal update involves local substitutions of the form $[0, 0]_p \leftrightarrow [1, b]_p$ and is attempted consecutively for every $p \in \{1, \dots, L\}$ in the sequence for which $[a, b]_p = [0, 0]_p$ or $[1, b]_p$. The updates are accepted with probabilities

$$\begin{aligned} P([0, 0]_p \rightarrow [1, b]_p) &= \frac{N\beta M_{1,b}(p)}{L-n}, \\ P([1, b]_p \rightarrow [0, 0]_p) &= \frac{L-n+1}{N\beta M_{1,b}(p)}, \quad (\text{A7}) \end{aligned}$$

where

$$M_{a,b}(p) = \langle \zeta_b(p), \zeta_{b+1}(p) | H_{a,b} | \zeta_b(p-1), \zeta_{b+1}(p-1) \rangle \quad (\text{A8})$$

is a matrix element on bond b , which in this case is diagonal ($a = 1$). Only a single state $|\alpha(p)\rangle$ is stored in the computer during the diagonal update. When off-diagonal operators are encountered during the successive scanning of the operator string, the corresponding electron states are updated so that the information needed for evaluation of the probabilities (A7) is always available when needed.

The operator-loop update has been discussed in detail in Ref. 17 in the context of spins. Here we present the construction of loops for fermions. As explained in Ref. 17, the matrix element in Eq. (A5) can be graphically represented by a set of n vertices (corresponding to the n non-unit operators in S_L) connected to one another by the propagated electron states. Each vertex has four “legs” with electron states $|\zeta_i(p-1), \zeta_{i+1}(p-1)\rangle$ and $|\zeta_i(p), \zeta_{i+1}(p)\rangle$ before and after the action of the associated Hamiltonian operator H_{a_p, b_p} . There are 32 allowed vertices – 16 diagonal ones and 8 each associated with the off-diagonal $H_{2,b}$ and $H_{3,b}$. A configuration (α, S_L) is completely specified by the leg states of the n vertices – except for sites that do not have any operators acting on them.

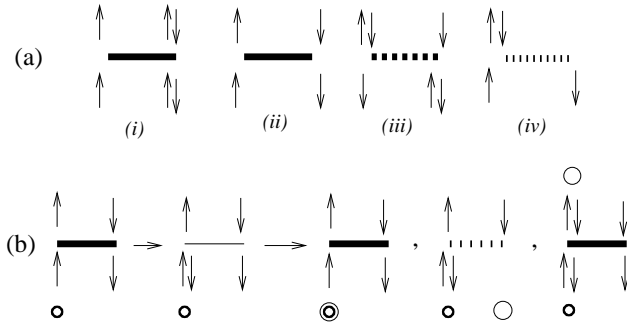


FIG. 11. (a) A few allowed vertices. The solid lines denote the diagonal Hamiltonian operator, the dashed and dotted lines denote the hopping operators for the up and down spins respectively. The lower legs denote the states $\zeta_i(p-1)$ and $\zeta_{i+1}(p-1)$ while the upper legs denote $\zeta_i(p)$ and $\zeta_{i+1}(p)$. (b) An example of a vertex update. The entrance leg is the lower left leg of the vertex, as indicated by the dot. The electron state at the entrance leg, \uparrow , is changed to $\uparrow\downarrow$ in this particular update. Given that, the 3 possible resulting vertices are shown. The corresponding exit legs are denoted by open circles. Exit at the upper right leg does not result in an allowed vertex in this case.

To carry out the operator-loop update, the linked list of the n vertices is first constructed. In addition to the electron states at the legs of each vertex, the list also contains the addresses (i.e., the location in S_L) of the next vertex and the corresponding leg that each leg is connected to. The loop construction begins with randomly choosing a vertex and an “entry” leg. The electron state at the entry leg is changed to one of the 3 other allowed states chosen at random. Next an “exit” leg is chosen (following a procedure described below) and its associated electron state is updated so that the new leg states constitute an allowed vertex. The exit leg will be linked to a leg of another vertex (or, if there is only one operator in the configuration which acts on the site in question, another leg on the same vertex) and this will be the entry leg for the next vertex. The electron state at this new entry leg is then updated to match the state at the exit leg of the previous vertex. A new exit leg is then chosen following the same procedure. This is repeated until the exit leg from a vertex points to the starting point of the loop, which implies that the loop is closed and a new allowed configuration has been generated.

To choose an exit leg — given a vertex, an entry leg and the updated electron state at the entry leg — all the legs can be considered in turn and attempts made to update the associated electron state so that the new leg states constitute an allowed vertex. Because of spin and charge conservation on the vertices, at a given exit leg there is at most one possible update of the electron state that can lead to an allowed vertex. Hence, the exit leg uniquely determines the new vertex and the probability of choosing a given leg should be proportional to the weight of the new vertex, i.e., a matrix element of the form (A8), which in this case can be either diagonal

or off-diagonal. In practice, a fast selection of an exit leg and updating of the vertex state is achieved using two pre-generated tables. The first one contains the cumulative probabilities of the 4 exit legs given an entrance leg, the old vertex state, and the new state at the entrance. The second table contains the new vertex states corresponding to the updated entrance and exit legs.

A special case occurs if the initial update at the entry leg of the first vertex of a loop is a spin-flip, i.e. the electron state changes from \uparrow to \downarrow or vice versa. In this case, the vertex weight does not change when updated and as a consequence the “bounce process”, where the exit leg is the same as the entrance leg, does not have to be included in the loop construction. The loop then becomes deterministic, i.e., there is a unique exit leg given the entrance leg.¹⁷

A full Monte Carlo updating cycle (MC step) consists of a diagonal update, followed by the construction of a linked vertex list. Next a number of operator-loop updates are carried out and finally the vertices are mapped back into a corresponding sequence S_L . The loop update typically also implies changes in the stored state $|\alpha\rangle = |\alpha(0)\rangle$, as some of the vertex legs (links) span across the periodic boundary in the propagation direction. The number of up and down electrons can be changed by the operator-loop update, as can the spatial winding numbers, and the algorithm is hence fully grand canonical. Note that at high and moderately low temperatures there are typically some sites of the system which has no vertices associated with them. The states on these sites can be randomly changed, since they have no affect the configuration weight.

The number of loops constructed for every MC step is determined such that on an average a total of $\sim L$ vertices (we typically use $2L$) are visited. The truncation L and the number of loops are adjusted during the equilibration part of the simulation and are thereafter held fixed. L is determined by requiring that the highest n reached during equilibration is at most 70 – 80% of L .

In certain parameter regions the length of a loop can sometimes become extremely long before it closes — it may even never close. It is therefore necessary to impose a maximum length, beyond which the loop construction is terminated and a new starting point is chosen (typically, we use $10L$ for this cut-off length). In order to reduce the likelihood of the next loop also exceeding the termination length it is useful to carry out a diagonal update before starting the next loop. The loop termination does not violate detailed balance and does not cause any systematical errors in the results. In most cases, incomplete loop termination occurs so infrequently that it does not adversely affect the simulation. In analogy with Ref. 34, the end points of the loop during construction can be related to the single-particle Green’s function of the system and hence the tendency for loops to become exceedingly long for some parameter values must be related to some physical properties of the system. This issue should be studied further.

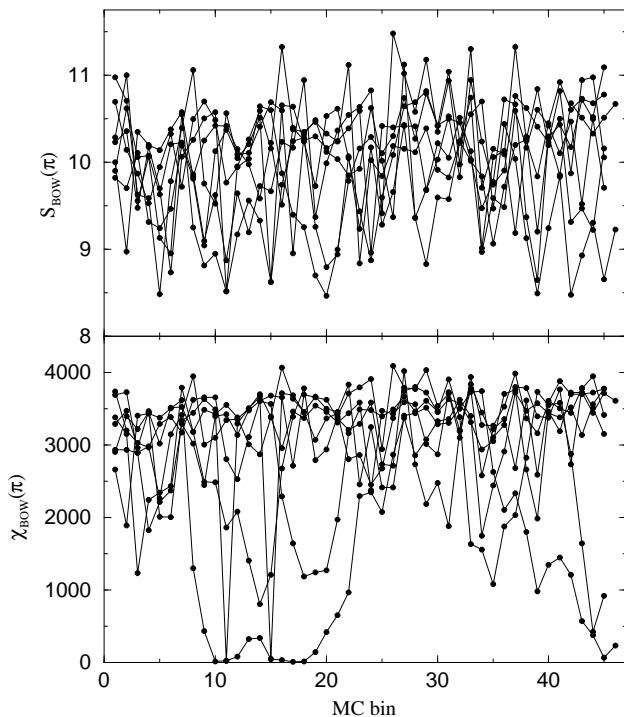


FIG. 12. The BOW structure factor and susceptibility for a 256-site system with $U = 4.0$ and $V = 2.14$ at inverse temperature $\beta = 512$. Results of six independent simulations are shown. Each point represents an average over a bin consisting of 10^4 Monte Carlo steps.

Estimators for the various structure factors and susceptibilities have been discussed in previous articles.^{15,16} The charge and spin stiffness constants, Eq. (6), can be expressed in terms of spin and charge current operators in analogy with the spin stiffness of the Heisenberg anti-ferromagnet previously discussed in Ref. 16, leading to

$$\rho_{c,s} = \frac{[(n_R^\uparrow - n_L^\uparrow) \pm (n_R^\downarrow - n_L^\downarrow)]^2}{N\beta}, \quad (\text{A9})$$

where $n_{R,L}^\sigma$ are the number of kinetic energy operators in the SSE term propagating spin- σ particles in the “right” and “left” direction on the ring. Because of spin and charge conservation, the topological winding numbers $(n_R^\sigma - n_L^\sigma)/N$ can take only integer values.

Although the operator-loop algorithm very significantly speeds up SSE simulations, in many cases reducing the autocorrelation function by orders of magnitude, the dynamics is still very slow for some parameter values. For the extended Hubbard model studied here, problems with very long autocorrelation times occur in the long-range ordered BOW and CDW phases. The problems are particularly severe for large systems close to the BOW-CDW phase boundary, where “trapping” in the wrong phase often occurs. The slow dynamics in the BOW phase is illustrated in Figure 12, which shows the simulation time dependence of $S_{BOW}(\pi)$ and $\chi_{BOW}(\pi)$ during a simulation of a 256-site system at $\beta = 512$ [S_{BOW} has converged

at this β but χ_{BOW} is about 20% larger still at $\beta = 1024$]. It is evident that the BOW autocorrelation function here is tens of thousands of MC steps. The BOW susceptibility exhibits a behavior where it sometimes takes very small values (less than 10^{-3} of the average value), but corresponding large fluctuations upwards do not occur, i.e., the distribution of the $\chi_{BOW}(\pi)$ estimator for individual configurations is very skewed. The structure factor exhibits a more symmetric distribution. This behavior can be understood as a consequence of the BOW ground state for a finite system being a symmetric combination of the two possible real-space symmetry-broken states. The symmetry is not broken in a finite system and the simulation is also not trapped in one of the real space-states. Hence, the wave function that is sampled in the simulation contains both the real-space states and, as will be argued below, the behavior seen in Fig. 12 indicates that individual configurations also contain both components, in such a way that transitions between the two real-space states can occur during the SSE propagation (which can be simply related³⁵ to a propagation in imaginary time). The susceptibility is an integral of the bond-order correlation, as in Eq. (4), which in configurations where tunneling occurs can be much smaller than in configurations with no tunneling, since correlations between states with the same real-space configuration contributes positively but correlations between different states give a negative contribution. The structure factor, on the other hand, is an equal time correlation function and would not be much reduced by tunneling if the tunneling times are short. This explains the qualitatively different distributions of the χ_{BOW} and S_{BOW} measurements in Fig. 12. Evidently, the updating process is very slow in adding and removing tunneling events in the configurations, which maybe is not that surprising considering that the tunneling is between two states with a discrete broken symmetry. These problems do not occur in SSE simulations of systems with a broken continuous symmetry, such as the two-dimensional Heisenberg model.

The trapping and tunneling problems can be significantly reduced by using the parallel tempering scheme, which is discussed below in Appendix B.

APPENDIX B: QUANTUM PARALLEL TEMPERING

The “quantum parallel tempering” scheme is a straight-forward generalization of the thermal parallel tempering^{18–20} method commonly used to equilibrate classical spin glass simulations. Our implementation amounts to running several simulations simultaneously on a parallel computer, using a fixed value of U and different closely spaced values of V at and around the critical value V_c . Along with the usual Monte Carlo updates, we attempt to swap the configurations for processes with

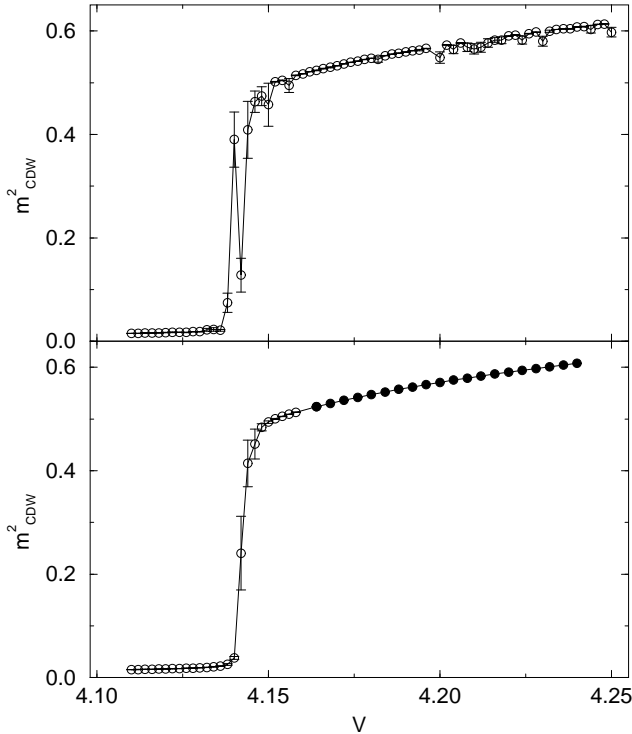


FIG. 13. The CDW order parameter across the CDW-SDW phase boundary for $U = 8.0$ ($N = 64$, $\beta = 64$). The upper panel shows data from individual runs. The lower panel shows the same data obtained using quantum parallel tempering, with two independent runs as indicated by the open and solid circles.

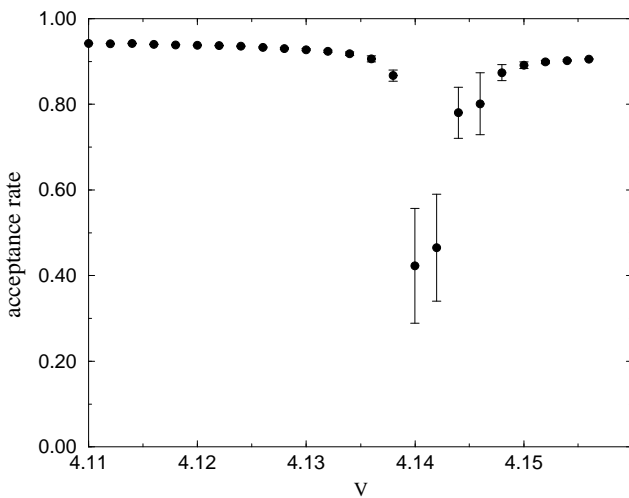


FIG. 14. The tempering acceptance rate during the simulation across the first-order SDW-CDW phase boundary.

adjacent values of V at regular intervals, typically after every Monte Carlo step, according to a scheme that maintains detailed balance in the extended ensemble of parallel simulations. The probability of swapping the V -values of runs i and $i + 1$, which are running at V_i and V_{i+1} , respectively, before the swap, is

$$P_{\text{swap}}(V_i, V_{i+1}) = \min\left[1, \frac{W_i(V_{i+1})W_{i+1}(V_i)}{W_i(V_i)W_{i+1}(V_{i+1})}\right], \quad (\text{B1})$$

where $W_i(V)$ is the weight of the i th simulation configuration evaluated with the coupling V . The swap probabilities for fixed $\Delta V = V_{i+1} - V_i$ decreases with increasing system size and decreasing temperature and hence ΔV and the range of V -values (if the number of processes is fixed) must be chosen smaller for larger system sizes.

The computational effort required for the swapping process is very minor compared to the actual quantum Monte Carlo simulations. It is therefore useful to carry out several swap attempts of all pairs of neighboring simulations between every MC step. Histograms containing the number of times each of the current configurations has “occupied” each V -bin can then be constructed and used for adding the contributions of each configuration to all the V -bins. This can contribute to reducing the statistical error of measured quantities.

To illustrate the advantage of quantum parallel tempering, we show two sets of data — obtained with and without the use of tempering — for a system undergoing a first order transition. Fig. 13 shows the CDW order parameter across the first-order CDW-SDW phase boundary at $U = 8.0$. The upper panel shows the data obtained from individual runs; the lower panel shows data for the same parameters obtained using tempering. The length of the individual simulations was 10^5 MC steps for all V values, and this was also the number of steps performed by each process in the tempering runs. The improvement in the quality of the tempering data is evident, especially close to the transition point where two of the individual simulations have relaxed into the wrong phases. The statistical errors are hence severely underestimated due to the failure to equilibrate properly within the simulation time. The tempering error bars are also large at the transition point, but in contrast to those of the individual simulations they can be expected to be accurate error estimates. The errors rapidly become much smaller as one moves away from the transition point. The effects of tempering are also favorable further inside the CDW phase, where several of the individual simulations are apparently affected by trapping in configurations with defects, where the order is reduced.

The tempering acceptance rate during the tempering run spanning across the phase transition in Fig. 13 is shown in Fig. 14. There is a sharp reduction in the acceptance rate at the transition. This reflects the rapid change in the SSE configurations across the phase boundary, which implies that the configuration weights evaluated with V values from the “wrong” phase are likely to

decrease and the swap according to the probability (B1) to be rejected.

Finally, we note that tempering, in general, is an application where a superlinear speed-up can be achieved in practice on parallel computers. In addition to doubling the density of data points when the number of processes is doubled, the statistical errors are also reduced. Sometimes the error reduction can be dramatic, but even in cases where there are no real problems with the dynamics of individual simulations the effects of tempering are often very favorable.

-
- ¹ V. J. Emery, S. A. Kivelson and O. Zachar, Phys. Rev. B **56**, 6120 (1997).
- ² H. G. Keiss (ed.), *Conjugated Conducting Polymers*, (Springer-Verlag, Berlin, 1992).
- ³ T. Ishiguro and K. Yamaji, *Organic Superconductors*, (Springer-Verlag, Berlin, 1990).
- ⁴ E. H. Lieb and F. Y. Wu, Phys. Rev. Lett. **20** 1445 (1968).
- ⁵ V. J. Emery, in *Highly Conducting One-Dimensional Solids*, ed. J. T. Devreese, R. Evrand and V. van Doren, (Plenum, New York, 1979), p.327.
- ⁶ J. Sólyom, Adv. Phys. **28**, 201 (1979).
- ⁷ J. E. Hirsch, Phys. Rev. Lett. **53**, 2327 (1984).
- ⁸ J. E. Hirsch, Phys. Rev. B **31**, 6022 (1985).
- ⁹ J. W. Cannon and E. Fradkin, Phys. Rev. B **41**, 9435 (1990).
- ¹⁰ J. W. Cannon, R. T. Scalettar and E. Fradkin, Phys. Rev. B **44**, 5995 (1991).
- ¹¹ P. G. J. van Dongen, Phys. Rev. B **49**, 7904 (1994).
- ¹² B. Fourcade and G. Spronken, Phys. Rev. B **29**, 5096 (1984).
- ¹³ J. Voit, Phys. Rev. B **45**, 4027 (1992).
- ¹⁴ M. Nakamura, J. Phys. Soc. of Japan **68**, 3123 (1999), Phys. Rev. B **61**, 16377 (2000).
- ¹⁵ A. W. Sandvik and J. Kurkijärvi, Phys. Rev. B **43**, 5950 (1991); A. W. Sandvik, J. Phys. A **25**, 3667 (1992).
- ¹⁶ A. W. Sandvik, Phys. Rev. B **56**, 11678 (1997).
- ¹⁷ A. W. Sandvik, Phys. Rev. B **59**, 14157 (1999).
- ¹⁸ E. Marinari, Lecture Notes in Physics, Vol. 501 *Advances in computer simulation: lectures held at the Eötvös Summer School in Budapest, Hungary, 16-20, July 1996*, edited by J. Kertész and I. Kondor (Springer, 1998).
- ¹⁹ K. Hukushima, H. Takayama, K. Nemoto, Int. J. Mod. Phys. C **7**, 337 (1996)
- ²⁰ K. Hukushima, K. Nemoto, J. Phys. Soc. Jpn. **65**, 1604 (1996)
- ²¹ P. V. Shevchenko, A. W. Sandvik, and O. P. Sushkov, Phys. Rev. B, **61**, 3475 (2000).
- ²² S. Wessel, B. Normand, M. Sigrist and S. Haas, cond-mat/0007228.
- ²³ W. Kohn, Phys. Rev. **133**, A171 (1964).
- ²⁴ Strictly speaking, our boundary conditions are antiperiodic, which is what one automatically obtains at half-filling when the system size N is a multiple of 4 and the fermion anticommutation relations giving negative signs from transport across the boundary are neglected.
- ²⁵ J. Voit, Rep. Prog. Phys. **57**, 977 (1994)
- ²⁶ R. T. Clay, A. W. Sandvik and D. K. Campbell, Phys. Rev. B **59**, 4665 (1999).
- ²⁷ H. J. Schulz, Phys. Rev. Lett. **77**, 2790 (1996).
- ²⁸ The logarithmic corrections typical for 1D systems make it very difficult to observe numerically that $\pi S_{SDW}(q)/q$ becomes exactly 1 [for a similar case, see: F. Woynarovich and H.-P. Eckerle, J. Phys. A **20**, L97 (1987)]. Empirically we have found that in the gapless case the value 1 is always approached from above, and hence the detection of the spin gap using this quantity is not hampered by the log-corrections — if $\pi S_{SDW}(q)/q$ decays below 1 one can conclude that here is a gap. Of course, one cannot strictly prove that the system is gapless if $\pi S_{SDW}(q)/q$ stays above 1, since for a very small gap the approach to 0 may occur only for q smaller than the smallest q of the largest system that can be studied.
- ²⁹ Strictly speaking, for a Kosterlitz-Thouless transition, exactly on the boundary the spin stiffness should approach a constant value as $N \rightarrow \infty$, with logarithmic size-corrections: H. Weber and P. Minnhagen, Phys. Rev. B **37**, 5986 (1987); K. Harada and N. Kawashima, J. Phys. Soc. Jpn. **67**, 2768 (1998).
- ³⁰ A. W. Sandvik and D. K. Campbell, Phys. Rev. Lett. **83**, 195-198 (1999).
- ³¹ K. Nomura and K. Okamoto, J. Phys. A **27**, 5773 (1994).
- ³² J. L. Cardy, J. Phys. A **20**, L891 (1987).
- ³³ W. P. Su, J. R. Schrieffer, and A. J. Heeger, Phys. Rev. Lett. **42**, 1698 (1979); Phys. Rev. B **22**, 2099 (1980).
- ³⁴ N. V. Prokof'ev, B. V. Svistunov, and I. S. Tupitsyn, Zh. Eks. Teor. Fiz. **64**, 853 (1996); Sov. Phys. JETP **87**, 310 (1998).
- ³⁵ A. W. Sandvik, R. R. P. Singh, and D. K. Campbell, Phys. Rev. B **56** 14510 (1997).